Calculation and experimental verification of force-magnetic coupling model of magnetized rail based on density functional theory

Minglun Li[a], HanYao[b,*],Jiarui Feng [a], Entao Yao[a], Ping Wang[a], Yu Shi[a]
[a]College of Automation Engineering, Nanjing University of Aeronautics and Astronautics, Nanjing 211106, China
[b]Department of Physics and Astronomy, University College London, Gower Street, London WC1E 6BT, United Kingdom
* Correspondence: ucapyao@ucl.ac.uk

Abstract: Metal magnetic memory(MMM) technology is one of the widely used non-destructive electromagnetic detection technology. However, the analysis of its underlying principle is still insufficient. The mechanical and magnetic coupling model is a reasonable standpoint to study the principle of MMM. In this paper, a mechanical and magnetic coupling model of steel material is established based on density functional theory (DFT) using the First-Principles analysis software CASTEP. In order to simulate the practical working scene, the residual magnetism in the rail is assumed to be existing and changing with the stress on the rail. By applying different stress to the model, we explored the relationship among the atomic magnetic moment, the lattice constant and the stress and further the causes of magnetic signals in the stress concentration zone. It is revealed that the atomic magnetic moment and the crystal volume decrease with the increase of compressive stress. The magnetic signal on the surface of magnetized metal component decreases with compressive stress increasing while the tensile stress shows opposite tendency. Generally speaking, the change of atomic magnetic moment and crystal volume caused by lattice distortion under stress can be seen as the fundamental reason for the change of magnetic signal on the surface of the magnetized metal. The bending experiment of rail shows that the normal magnetic field decreases with the increase of compressive stress in the stress concentration zone. The conclusion is verified by experiments.

Keywords: First-Principles, force-magnetic coupling, stress detection, Non-destructive electromagnetic detection technology

1 Introduction

Rails in use are continuously squeezed and worn by wheels, resulting in stress concentrations. If not detected in time, cracks and other significant damages are more likely to arise[1]. For example,

according to the statistics from the Canadian government, 82 railway accidents occurred in January 2020 alone, including derailment[2]. In recent years, nondestructive testing technology for rail cracks and early damages are developing rapidly, partially including magnetic flux leakage testing technology and Barkhausen noise detection technology[3][4]. Due to the reflection clutter near the surface of the rail, the ultrasonic testing technology can only detect large defects inside the rail, which makes the rail surface or near-surface becomes the blind area, and thus a potential safety hazard. Eddy current testing technology can quickly detect the rail surface without adding a coupling agent. However, due to the limitation of skin effect, eddy current testing can only detect the opening defects on the surface, but cannot detect the buried defects near the surface. Magnetic flux leakage testing technology has the advantages of fast detection speed, low cost and simple operation, and it can detect both surface cracks and buried cracks of rail. However, it is difficult to detect the deep buried defects. Most of the current theoretical analyses of magnetic signals of the magnetized metal use the finite element method for macroscopic simulation[5][6] which limits the further research of the physical mechanism.

Rail are usually under pressure due to the action of wheels. We abstract the rail detection into magnetized metal under changing pressure. In this paper, we use the First-Principles of quantum mechanics to explore the possible microscopic phenomena in the magnetized metal under changing pressure. Metal is a kind of crystal materials. It is a powerful tool in the field of computational materials to calculate the properties of crystal materials, such as optical properties, acoustic properties, magnetic properties[7]. Theoretically, this calculation requires solving the Schrödinger equation for a multi-particle system. However, the complexity of the system makes it unrealistic and the density functional theory (DFT) was proposed for approximation and reduction of the calculative load[8].At present, LDA (local density approximation) and GGA (generalized gradient approximation) are commonly used. LDA is a class of approximations to the exchange-correlation (XC) energy functional in DFT that depend solely upon the value of the electronic density at each point in space. The LDA assumes that the density is the same everywhere. Because of this, the LDA has a tendency to underestimate the exchange energy and over-estimate the correlation energy. The errors due to the exchange and correlation parts tend to compensate each other to a certain degree. To correct for this tendency, it is common to expand in terms of the gradient of the density in order to account for the non-homogeneity of the true electron density. This allows corrections based on the changes in density away from the coordinate. These expansions are referred to as GGA.

First-Principles is a basic proposition or assumption and have been used to calculate the influence of external force field and doping effect on the material magnetic memory characteristics but its related researches are more focused on the development of new steel alloys[9] or metal magnetic memory(MMM) technology[10]. The principle of MMM detection is based on the fact that the magnetic domain would be reoriented and irreversible in the stress and deformation concentrated area under the combined action of the working load and the earth's

magnetic field. The invertibility of the magnetic state will remain after the removal of the working load. It also be related to the maximum acting force. In other words, the MMM corresponding to the acting stress will be generated[11]. The theory of metal magnetic memory lacks the force-magnetic coupling model. In this paper, the rail is taken as the research object, and the force-magnetic coupling model is established based on the density functional theory for the rail steel material under general magnetization. The stress-magnetic relation of steel material under magnetization is analyzed in the following section and experimental verification are given in the third section.

2 Establishment and optimization of the model

In order to study the physical mechanism of the MMM, it is necessary to calculate the parameters associated with the magnetic characteristics of steel materials under different stresses, i.e., the changes of crystal volume, atomic magnetic moment and density of electronic state[12][13]. The CASTEP software module is used here for modeling and calculation.

At present, rail steels, which are usually low carbon steel, are composed of pearlite and bainite **错误!未找到引用源。**, whose lattices are all body-centered cubic (α - Fe structure). Therefore, the α - Fe crystal structure without carbon doping is chosen to explore the rule of changes of magnetic characteristics under stress.

The α - Fe structure is classified as an A2 type atom stacking mode. The iron atoms are tightly packed in the cube, which means its space group is Im3m. Figure 1 shows the crystal cell which is used in this paper.

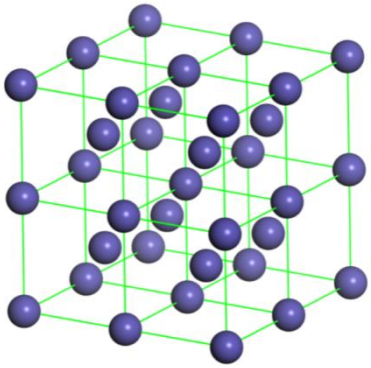

Figure 1. 8α-Fe cell

The cut-off energy of the plane wave basis function and the K-point in the Brillouin zone are optimized in advance. The cut-off energy is one of the parameters of inverse space, which corresponds to the size of each discrete unit in the real space after discretization. The selection of K-point in the Brillouin zone is equivalent to the refinement of meshing in K-space[8]. When the energy of the system is minimum and converges, the system will generally be stable. The following calculations are carried out to find the relationship between the system stability and two influencing factors, the cut-off energy and K-point.

Firstly, as shown in Figure 2, when the cut-off energy exceeds 350eV, the system energy tends to be stable and converges at -863.5eV. Then we select 4×4×4, 8×8×8, 10×10×10, 12×12×12, 16×16×16 of samples for the Brillouin area K- point. As shown in Figure 3, when 8×8×8 or higher is selected, the system energy tends to be constant. In this paper, a 450eV cut-off energy and 16×16×16 Brillouin K-points are selected to ensure accuracy and reduce the calculation time. For magnetic materials, spin polarization is considered. As shown in Figure 4, after 9 iterations, the total energy of the selected cell tends to become constant, indicating that the selected parameters are appropriate.

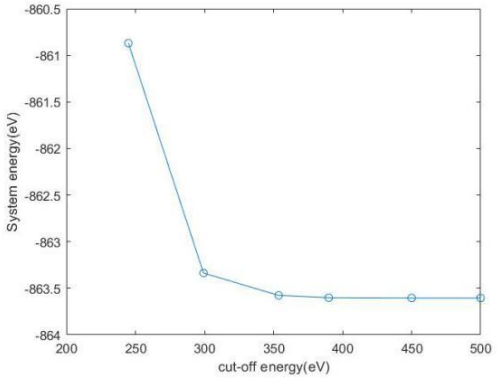

Figure 2. System energy under variable cut-off energy, when the cut-off energy exceeds 350ev, the system energy tends to be stable and converges

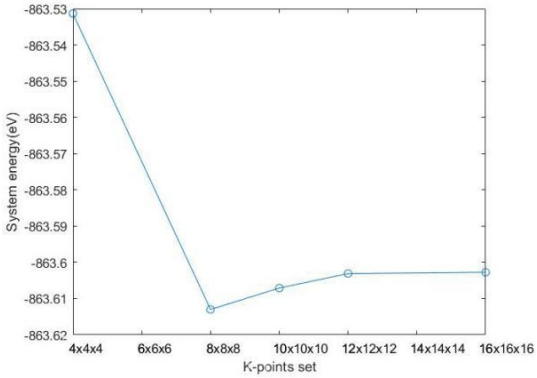

Figure 3. System energy under variable K-points set, when 8 × 8 × 8 or higher is selected, the system energy tends to be constant

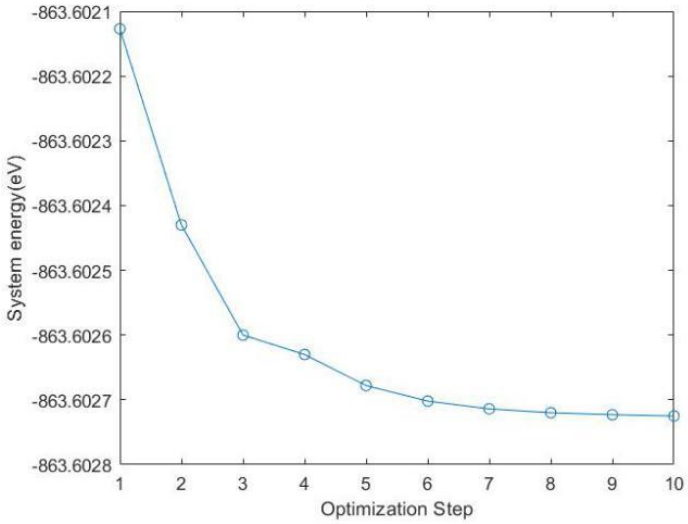

Figure 4. Process of system energy becoming stable with multiple optimization steps

The energy convergence of the optimized model can only indicate that the model is self-consistent. For more accuracy, it is necessary to compare the model with experimental data of references[15][16]. Table 1 shows a comparison between the calculated data and standard previous experimental data. Among all the listed, the idea of Local Density Approximation (LDA) is to replace non-uniform electron gas with uniform electron gas approximately, while Generalized

Gradient Approximation (GGA) introduces electron density gradient, which not only considers the approximation of local electron density, but also considers the spatial heterogeneity of electron density, which is much more accurate compared with LDA algorithm. PW91, PBE, RPBE are the three most typical and popular exchange functionals[17].

It can be seen from Table 1 that the lattice constants and atomic magnetic moments calculated by the GGA method are closer to the standard previous experimental data than those calculated with the LDA method. In this paper, the GGA-PW91 is used to calculate the relationship between stress and the magnetic signal of rail steel in a magnetization state.

Table 1 Comparison of theoretical and experimental parameter of different methods and functional

Method	Lattice constant of the cell/ $\times 10^{-10}$m	Atomic magnetic moment of the cell (μ_B/atom)	Deviation from the experimental value of lattice constant/ $\times 10^{-10}$m	Deviation from the experimental value of atomic magnetic moment (μ_B/atom)
LDA-CAPZ	2.746	2.01	-0.064	-0.20
GGA-PW91	2.826	2.12	0.016	-0.09
GGA-PBE	2.834	2.09	0.024	-0.12
GGA-RPBE	2.890	2.10	0.080	-0.11
GGA-WC	2.783	2.04	-0.027	-0.17
GGA-PBESOL	2.784	2.03	-0.026	-0.18
Previous experimental data	2.810[15]	2.21[16]	-	-

The atomic magnetic moment, unit-cell volume and magnetic induction intensity were used to established the microscopic cell model of rail steel in CASTEP. The stacking mode is A2 type, with 450eV as the cut-off energy, 16×16×16 as the k-point of Brillouin zone, and PW91 functional of GGA method as the approximation method. Without magnetization, the lattice constant is 2.826 $\times 10^{-10}$m and the atomic magnetic moment is 2.12 μ_B / atom, where μ_B refers to Bohr magneton.

The First-Principles module CASTEP is used to calculate the atomic magnetic moment, cell volume of ferromagnetic crystal and the relationship between these parameters and stress.

According to Stoner's theorem, the net magnetic moment of ferromagnetic material is the sum of the atomic magnetic moments of all particles in the material. The net magnetic moment of the system increases with the external magnetic induction intensity increasing. Its expression is:

$$\vec{P}_m = \sum_i \vec{\mu}_i \tag{1}$$

where $\vec{P}_m$ is the net magnetic moment of the whole material and $\vec{\mu}_i$ is the atomic magnetic moment of each particle.

If the volume of the material is V , the magnetization M_r of the material can be expressed as:

$$M_r = \frac{d\vec{P}_m}{dV} \tag{2}$$

The magnetic signal discussed in this paper is generated under the condition of magnetization. Therefore, the total magnetic induction intensity *B* is the sum of the magnetic induction intensity of the material of the surrounding and the magnetic induction intensity B_1 generated by the material itself:

$$B = B_0 + B_1 \tag{3}$$

where B_0 is the magnetic induction intensity of the material generated by the earth. Also, considering:

$$B_0 = \mu_0 H \tag{4}$$

where μ_0 is the free space permeability and H is the external magnetic field intensity B_1 can be expressed as:

$$B_1 = \mu_0 M_r \tag{5}$$

Then:

$$B = \mu_0 (H + M_r) = \mu_0 (H + \frac{d\sum_i \vec{\mu}_i}{dV}) \tag{6}$$

where M_r is the magnetic moment per unit volume. It can be deduced from Formula (6) that *B* has a monotonic positive correlation with M_r. According to formula (6), the relationship between the magnetic signal and the stress can be obtained by calculating the variation law of the atomic magnetic moment, the crystal volume and the stress.

The calculation results are shown in Figure 5. With the increase of tensile stress, the atomic magnetic moment of α - Fe crystal cell increases. With the increase of the compressive stress, the atomic magnetic moment of the α - Fe cell decreases. In addition, crystal volume is also calculated, which is shown in Figure 6. The volume of the crystal is calculated from the lattice constant. It can be seen that with the increase of compressive stress, the volume of crystal cell decreases, and the speed of reduction slows down gradually, which means that the compressive stress makes the crystal structure denser.

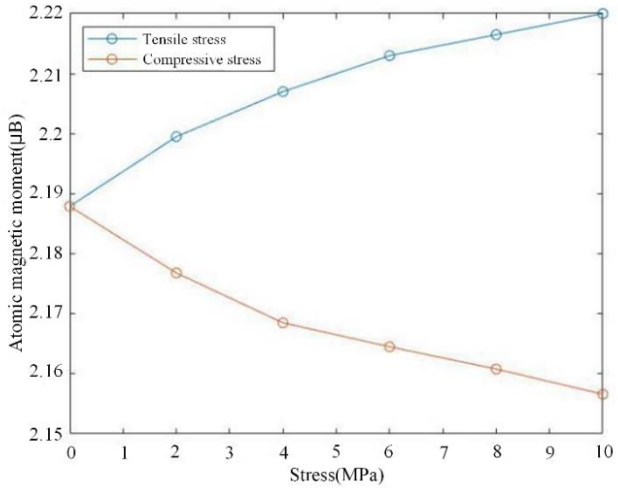

Figure 5. Calculation results: variation trend of atomic magnetic moment with stress

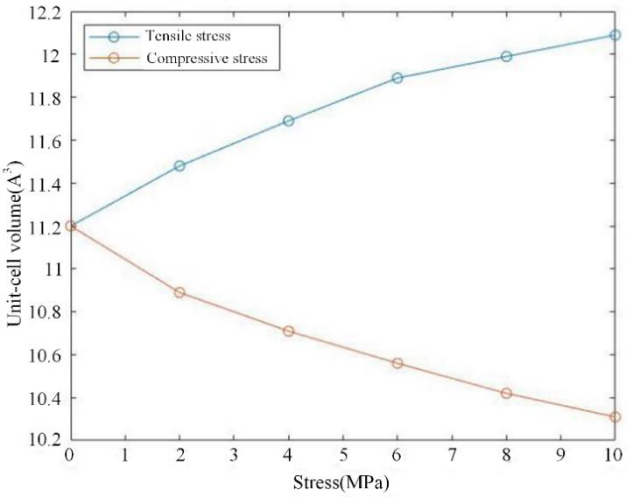

Figure 6. Calculation results: variation trend of crystal volume with stress

A cell is taken as an object and an external magnetic field B_0=1T is applied as along the direction of the magnetized cell. Then by introducing the calculation results of figure 5 and figure 6 into formula (6), the relationship between stress and magnetic induction of magnetized steel can be deduced, as shown in Figure 7.

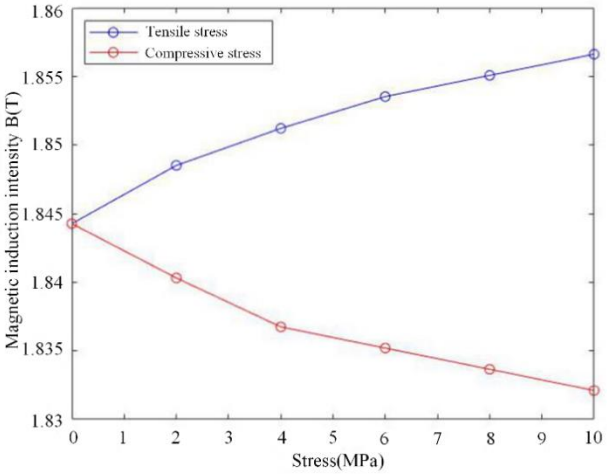

Figure 7. Calculation results: variation trend of magnetic induction with stress

When the material is stretched, the lattice constant of the crystal in the direction of stress is higher when compared with the equilibrium state. And the atomic magnetic moment also increases. Similarly, when the material is under compressive stress, the lattice constant in the direction of the stress of the crystal decreases, and the atomic magnetic moment also decreases. If the change of lattice volume reaches the threshold, the bond between the Fe atoms breaks[18]. At this time, the lattice of the system becomes distorted, which will affect the magnetic characteristics of the material itself.

In the spin-polarized system, the density of electronic states are oriented according to the energy state. The difference in the populations reflects the magnetic strength of the material. If they are equal, that is, the electron density of states is symmetrically up and down, the material as a whole does not show magnetism, and the difference between the two affects the atomic magnetic moment and the material magnetism[19].

Figure 8 shows the electron density of state distribution of each orbit of the Fe atom in the α -Fe crystal cell when no stress is applied. Among them, the density of electronic states of s, p and f orbits are shown in Figure 8 (a), the density of electronic states of d orbits and the sum of each orbit are shown in Figure 8 (b). These two graphs use the same scales for easier comparison. It can be seen that the density of electronic states of the s, p and f orbitals are evenly distributed, and its peak value is far lower than that of the d orbitals. This shows that the spin motion of the d orbitals contributes most to the magnetic properties of the materials, and the contribution of the other orbitals to the magnetic properties can be ignored. Fe belongs to the group of 3d transition metals. Its ferromagnetism comes from the intrinsic magnetic moment produced by the spin motion of 3d orbital electrons in each Fe atom. The intrinsic magnetic moment tends to be parallel under the interaction, and produces the magnetic moment in a specific direction, that is, the macroscopic ferromagnetism.

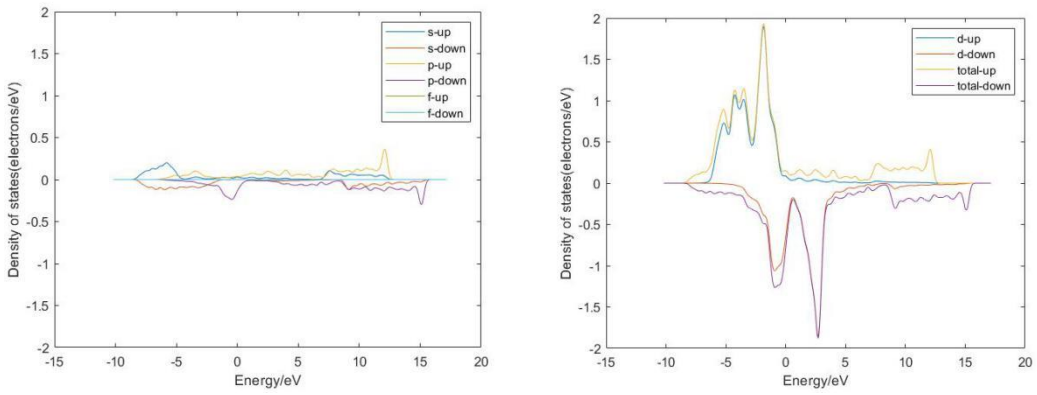

(a) (b)

Figure 8. Partial electron density of states of various orbits of Fe atom

Therefore, the simulation calculation and analysis show that the change in the magnetic signal is caused by the change in the atomic magnetic moment and lattice distortion under stress.

3 Experimental design, results and analysis

As are shown in Figure 9, a U71Mn (Chinese national standard) rail which was used for a long time and a stress loading device were used to carry out a rail stress loading test to verify the CASTEP calculations.

A Hall sensor is fixed on the free end of the cantilever which is driven by a piezoelectric actuator with sinusoidal voltage. The output of the sensor was a sine-wave signal, the amplitude of which was proportional to the normal magnetic field gradient. Since the normal magnetic field gradient depended only on the varying quantity of the magnetic field in the sweep range, the influence of the background magnetic field was neglected. The fundamental frequency of the alternating output signal of the Hall sensor is the frequency of the vibration. The signal was filtered, amplified and sent to the microcontroller to calculate the peak value. The magnetic sensor is shown in Figure 10.

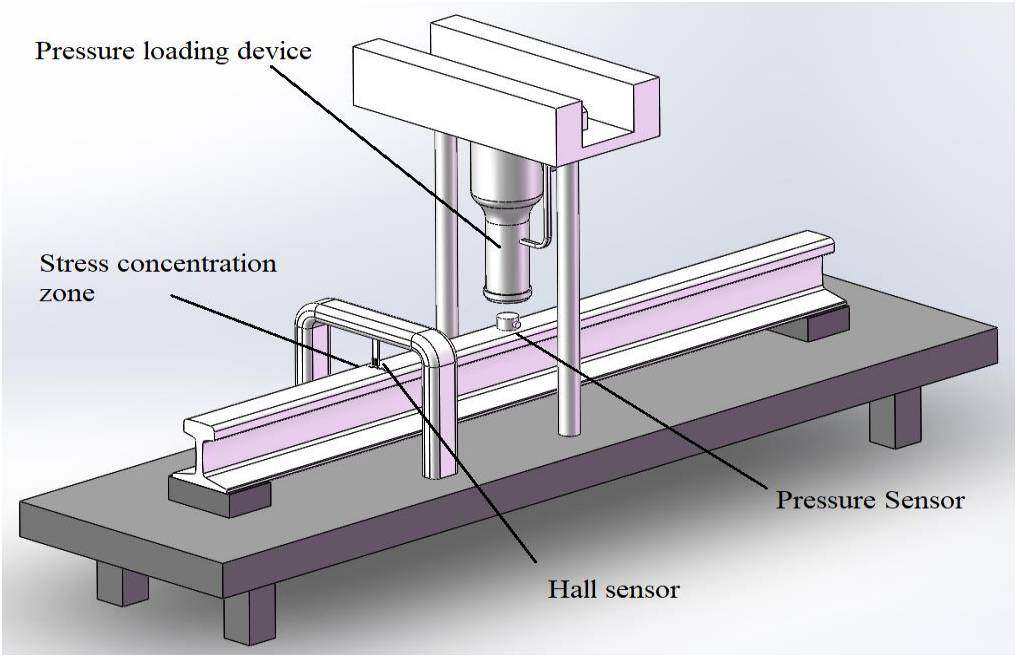

Figure 9. Diagram of the experimental rail sample and the stress loading device; There is a stress concentration zone around an artificial crack whose depth is 0.5mm and the width is 0.2mm.

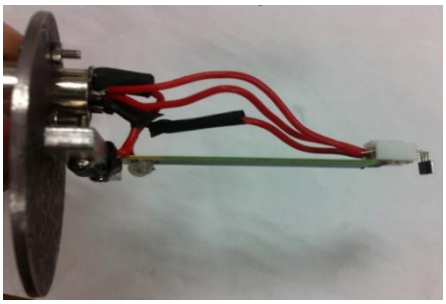

Figure 10. Magnetic sensor

The system works in dynamics and it includes a magnetic sensor, the vibration detection hardware circuit, a signal acquisition module and an upper computer human-computer interface. The data collected by the sensors were processed by their respective signal conditioning circuit, and then transmitted to the upper computer system by the acquisition card for analysis. Figure 11 shows schematics of the measurement system.

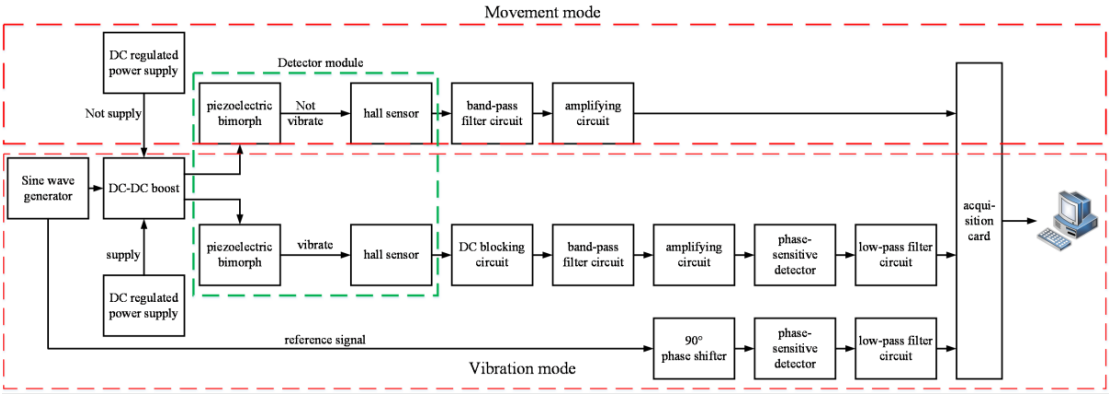

Figure 11. Schematic diagram of the inspection system; The sine wave generator provides a peak-to-peak value of 2V and a sinusoidal excitation signal with a frequency of 100Hz, thereby driving the piezoelectric bimorph vibration to drive the sensor to scan and detect the magnetic field, and as a reference signal together with the detection signal through the lock-in amplifier. The DC-DC boost amplifies the sinusoidal signal to a peak-to-peak value of 150V to drive the piezoelectric bimorph. The DC blocking circuit removes the DC component. The band-pass filter circuit extracts the 100Hz center frequency signal and amplifies it to improve the circuit quality factor Q, suppress noise interference, and greatly improve the signal-to-noise ratio. The amplifying circuit amplifies the signal again to meet the input requirements. The 90 °phase shift circuit processes the sinusoidal signal to obtain a reference signal with a phase difference of 90 °and provides it to the phase-sensitive detector. The phase-sensitive detector circuit completes the cross-correlation operation of the reference signal and the detection signal and extracts the useful detection signal from it. The Low-pass filter circuit removes high-frequency noise.

In a stress concentration zone, the position where the normal magnetic field B_n passes a zero point has the maximum gradient of the normal magnetic field. Therefore, the stress concentration is determined by the maximum of the normal magnetic field gradient. In addition, on the surface to which the stress concentration zone corresponds, the distribution curve of the normal magnetic field gradient is steeper than the curve of the normal magnetic field, the variety is more significant, it is much easier to detect by experiment. The measurement of the distribution of the normal

magnetic field suffers interference from the background geomagnetic field and the geomagnetic field is a constant, while the normal magnetic field gradient is the variation of the magnetic field over distance and can eliminate the interference from the background geomagnetic field. Therefore, the gradient is the more valid feature that characterizes damage than zero-crossings of the normal magnetic field.

The characteristic value of the magnetic detection signal can be characterized by the magnetic field intensity and the magnetic field gradient. In order to measure the magnetic field gradient, the Hall sensor is driven to vibrate with a given frequency and amplitude, and the peak-to-peak value of the sensor output signal was proportional to the gradient value of the magnetic field. Based on this method, the normal magnetic field gradient on the surface of the vibration scanning component was measured to represent the magnetic field intensity. The normal magnetic field gradient is the derivative of the normal magnetic field with respect to distance. The larger the normal magnetic field gradient, the larger the normal magnetic field at the same location.

To avoid electromagnetic interference, a piezoelectric bimorph was used to drive the magnetic sensor instead of the electromagnetic actuator. The sinusoidal signal with the fixed frequency was generated to drive the piezoelectric bimorph. The driving system includes a wave form generator, a DC regulated power supply, a DC-DC boost and a piezoelectric bimorph. The piezoelectric bimorph can bend if AC voltage is applied and then cause the Hall sensor to produce lateral displacement.

The piezoelectric bimorph structure in this paper was double-layered which was composed of two piezoelectric ceramic sheets and intermediate electrodes. The arrangement of the piezoelectric ceramic sheets was in the same polarization direction, and they were pasted on both sides of the intermediate electrode layer. If an AC power supply was adopted, an amplitude of the same frequency would be generated. It has the characteristics of fast response speed, small volume and high reliability. When the driving voltage is 150V, the swing amplitude can reach 1mm.

The displacement formula generated by the simple harmonic vibration of the sensor is

$$x = a\sin(2\pi ft) \tag{7}$$

In formula (7), a represents the vibration amplitude of the piezoelectric bimorph, f represents the vibration frequency of the sensor, which is of the same frequency as the driving signal, and x represents the displacement of the simple harmonic vibration of the sensor.

Assuming that the sensor output is $U=kB_n$, and k is the sensitivity coefficient of the sensor, the derivative of the output signal to time t is

$$\frac{dU}{dt} = \frac{d(kB_n)}{dt} = k \cdot \frac{dB_n}{dx} \cdot \frac{dx}{dt} = k \cdot G\left[a \cdot 2\pi f \cdot \cos(2\pi ft)\right] \tag{8}$$

where B_n is the normal magnetic field and G is the magnetic field gradient.

According to the formula (8), it can be seen that the normal magnetic field gradient is proportional to the amplitude of the applied cosine driven signal. Because the sensor output U reflected the magnetic field intensity, the derivative of U to time represents the magnetic field

gradient at a stress concentration zone when the sensor is in simple harmonic vibration. By superimposing it on the amplitude of a periodic sinusoidal signal, the output of the detection signal can be obtained according to formula (8) and the amplitude of the cosine signal is used to express the magnetic field gradient. In formula (8), given that f =100Hz, a = 1mm, and the sensor sensitivity is 1.35m*V/Gs*, the relationship between the sensor output amplitude A and the magnetic field gradient G can be obtained as follows:

$$A = k \cdot G \cdot a \cdot 2\pi f = 8.5 \times 10^{-4} \cdot G[V/(Gs/m)] \tag{9}$$

The force was applied to the rail sample to make it slightly bend. At this time, the compressive stress appears on the upper surface of the rail and the tensile stress appeared on the lower surface. The stress value near the magnetic sensor recorded with a pressure sensor. The compressive stress was increased from 15MPa to 150MPa, and then back to 15MPa. Five times of reciprocating were carried out. The trend of each magnetic signal was recorded, and the average value was calculated. Due to the size of the device, only the compressive stress experiment was carried out. It can be seen from the experimental results that the normal magnetic field gradient of rail surface magnetic signal decreases with the increase of compressive stress, which is consistent with the trend of CASTEP calculation and analysis.

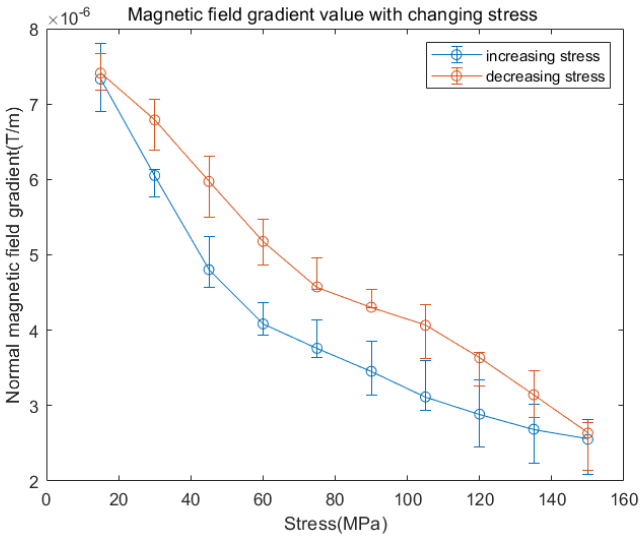

Figure 12. Magnetic field gradient with changing compressive stress

4 Conclusion

In this paper, the force-magnetic coupling model of MMM is explored and verified by simulation and experiment. CASTEP analyses suggests that three main reasons for the change of magnetic signal with stress in ferromagnetic materials after long-term magnetization. That is, the change of the electron spin density of states, the crystal volume and the band structure in ferromagnetic crystals. Both the relationship are established of atomic magnetic moment and crystal volume versus the stress and of the surface magnetic signal versus the atomic magnetic moment and crystal volume. The calculation and analysis show that the change in the magnetic signal is caused by the change in the atomic magnetic moment and lattice distortion under stress.

In order to verify these results, a stress loading device was set up and external stress was applied to a U71Mn (Chinese national standard) rail sample. The bending experiment of rail shows that the normal magnetic field decreases with the increase of compressive stress in the stress concentration zone. The experimental results proves the effectiveness of the force-magnetic coupling model for the explanation of MMM.

5 Acknowledgments

This paper is supported by the special programme for Key Scientific Instrument and Equipment Development of the Ministry of Science and Technology (No.2016YFF0103702), the National Natural Science Foundation of China (NO.62073162) and the Key Laboratory of Non-destructive testing and monitoring technology for high-speed transport facilities of the Ministry of Industry and Information Technology.

References

[1] Y Li, J J Chen and J X Wang, 'Analysis of Fatigue Crack Propagation in Rails Under Combined Action of Wheel Load and Residual Stress', Engineering Failure Analysis, Vol 115, pp 104689, September 2020.

[2] 'Transportation Safety Board of Canada. Monthly rail statistics for January 2020'. https://www.bst-tsb.gc.ca/eng/stats/rail/2020/01/r2020-01.pdf, 2020

[3] Y A Onur, 'Condition monitoring of Koepe winder ropes by electromagnetic non-destructive inspection', Insight, Vol 54, No 3, pp 144-148, March 2012.

[4] Y A Onur, H Gelen, 'Investigation on endurance evaluation of a portal crane: experimental, theoretical and finite element analysis', Materials Testing, Vol 62, No 4, pp 357-364, April 2020.

[5] J S Gao, Y Wei and H Chen, 'The Research on Defect Recognition Method for Rail Magnetic Flux Leakage Detecting', Proceedings of 2012 International Conference on Measurement, Information and Control, Vol 2, pp 745-750, August 2012.

[6] A Marek, B Augustyniak and L Piotrowski, 'Determination of Magnetisation Conditions in a Double-Core Barkhausen Noise Measurement Set-Up', Journal of Nondestructive Evaluation, Vol 34, No 2, pp 1-8, June 2015.

[7] G Z Qiu, Q Xiao, Y H Hu, W Q Qin and D Z Wang, 'Theoretical study of the surface energy and electronic structure of pyrite FeS2 (100) using a total-energy pseudopotential method, CASTEP', Journal of Colloid and Interface Science, Vol 270, pp 127-132, February 2004.

[8] W Kohn, 'Density Functional Theory for Systems of very Many Atoms', International Journal of Quantum Chemistry, Vol 56, No 4, pp 229-232, November 1995.

[9] J H Jang, C H Lee, Y U Heo and D W Suh, 'Stability of (Ti,M)C (M=Nb, V, Mo and W) carbide in steels using first-principles calculations', Acta Materialia, Vol

60, No 1, pp 208-217, January 2012.

[10] G Q Wang, P Yan, L W Wei and Z L Deng, 'The Magnetic Memory Effect of Ferromagnetic Materials in the Process of Stress-Magnetism Coupling', Advances in Materials Science and Engineering, Vol 2017, pp 1-8, August 2017.

[11] A A Doubov. 'Diagnostics of metal items and equipment magnetic by means of metal magnetic memory', Proceedings of CHSNDT 7th Conference on NDT and Internation Research Symposium, pp 181-187, 1999.

[12] A Hoda, A Ghorbanpoor and S Shams, 'Development of Robotic Nondestructive Testing of Steel Corrosion of Prestressed Concrete Bridge Girders using Magnetic Flux Leakage System', Transportation Research Record, Vol 2674, No 8, pp 466-476, June 2020.

[13] L B Shi, C Y Xu and H K Yuan, 'A CASTEP Study on Magnetic Properties of C-Doped ZnO Crystal', Physica. B, Condensed Matter, Vol 406, No 17, pp 3187-3191, September 2011.

[14] Z Yuan, Y T Zhai and Z Zhang, 'Analysis on the Frequency-Dependent Impedance of the Traction Network Based on Electromagnetic Parameters Measurement of the Steel Rail', 2019 4th IEEE Workshop on the Electronic Grid (eGRID), pp 1-5, 2019.

[15] D R Lide, 'CRC Handbook of Chemistry and Physics', CRC Press, Florida,1992.

[16] C Kittel, 'Introduction to Solid State Physics (5th Ed.)', Wiley, NewYork, 1976.

[17] P J A Ribeiro-Claro, P D Vaz, M M Nolasco and A M Amado, 'Understanding the Vibrational Spectra of Crystalline Isoniazid: Raman, IR and INS Spectroscopy and Solid-State DFT Study', Spectrochimica Acta. Part A, Molecular and Biomolecular Spectroscopy, Vol 204, pp 452-459, November 2018.

[18] Z H Yang, G L Liu, Y D Qu and R D Li, 'Electronic Mechanism of Dislocation and Doping for Impact Toughness of Ductile Cast Iron', Jisuan Wuli/Chinese Journal of Computational Physics, Vol 32, No 4, pp 482-486, July 2015.

[19] D S Dai and K M Qian, 'Ferromagnetism', Science Press, Beijing, 2017.